Predicting delamination of composite laminates using an imaging approach

Zhongqing Su[1,3], Li Cheng[1], Xiaoming Wang[2], Long Yu[1] and Chao Zhou[1]

[1] Department of Mechanical Engineering, The Hong Kong Polytechnic University, Kowloon, Hong Kong SAR
[2] Urban Systems Program, CSIRO Sustainable Ecosystems, Commonwealth Scientific and Industrial Research Organisation, 37 Graham Road, Highett, Melbourne VIC 3190, Australia

E-mail: MMSU@polyu.edu.hk

Abstract
The present work concerns the development of a Lamb-wave-based imaging approach with the capacity to visually pinpoint structural damage, if any, in terms of the probability of damage occurrence at all spatial positions of the structure under inspection. To establish such probabilities, individual sensors of an active sensor network contributed their perceptions as to the damage occurrence near them using the signal feature *time-of-flight* (ToF) extracted from captured Lamb wave signals. All these perceptions were then fused by virtue of an image arithmetic algorithm. The prediction results were presented in an image where the location and size of all the damage instances in the structure became intuitional, rather than provided with definitive damage parameters. Such a probability-based imaging approach is by nature more consistent with the implication of *prediction* or *estimation* of damage than traditional identification endeavours. The effectiveness of the approach was experimentally demonstrated by predicting delamination in carbon-fibre-reinforced epoxy (CF/EP) laminates.

(Some figures in this article are in colour only in the electronic version)

1. Introduction

Advanced composite structures have been increasingly employed in the new generation of jumbo aircraft to pursue significant weight saving and substantial performance improvement, exemplified by the latest models *Boeing 787* and *Airbus 350*, in which consumption of fibre-reinforced composite materials has reached unprecedented levels of 50% and 40%, respectively [1, 2]. As envisaged, the composite structures in aircraft are often subject to (i) low energy impacts caused by dropping tools or mishandling during manufacture, assembly or maintenance; (ii) medium energy impacts caused by foreign objects such as stones, hail or birds during service; or (iii) high energy impacts caused by military projectiles such as a bullet [3]. In case (i) only very slight indentation can be seen on the impact surface and this level of damage is referred to as *barely visible impact damage* (BVID); in case (ii) it is usually possible that local severe indentation is produced; and in case (iii) penetration occurs but the damaged area is generally small. In practice, fibre-reinforced composite laminates are prone to low and medium impacts, and as a result present delamination inside (appearing as debonding of adjoining plies) and fibre breakage on the opposite side of the laminate to the impact. The occurrence of delamination can considerably lower structural strength and thus reduce the reliability of aircraft.

The methods for evaluating delamination of fibre-reinforced composite laminates are legion, represented by approaches using structural dynamic responses, radioscopy, ultrasonic scanning, infrared thermography, eddy currents, impedance, etc [4–7]. Although developed on the basis of different mechanisms, the ultimate purpose of these approaches is identical: predicting the location and shape of delamination with definitive damage parameters (e.g. position, shape, orientation and size) as accurately as possible. However, determination of these definitive damage parameters can be in a highly subjective manner subject to individual operators, and erroneous estimation might arise if captured signals contain much uncertainty or present incompleteness.

---

[3] Author to whom any correspondence should be addressed.

In conjunction with the active sensor network technique, recently there has been increasing awareness of using the probability to describe a damage event [8–13], in line with the recognition that damage identification is an exercise to *predict* or *estimate* damage, and thus it is ideal to deliver the identification results in terms of the *probability* as to the occurrence of a damage event across the entire structure under inspection. Such a detection philosophy is in nature more consistent with the implication of *prediction* or *estimation* than traditional approaches are. In this process, the utility of an active sensor network is an important step towards the development of structures or systems with the capability of self-health-monitoring, so as to cater for the concept of a 'smart structure', which is defined as a structure endowed with one or more specific *built-in* functions to respond in certain manner [14]. The sensor network technology can be seen as a basic ingredient in today's efforts to develop smart structures and systems.

In this study, a Lamb-wave-based damage imaging approach was developed with the capacity to visually pinpoint structural damage, if any, in terms of the probability of damage occurrence at all spatial positions of the structure under interrogation. By virtue of an active sensor network, the prediction results were intuitively delineated in an image calibrated with the probability of damage existence. The image is able to reveal the overall health status of the entire structure under inspection. The approach was experimentally validated by predicting single and dual delamination in carbon-fibre-reinforced epoxy (CF/EP) laminates, respectively.

2. Damage identification using time-of-flight (ToF) extracted from Lamb wave signals

2.1. Lamb waves

Lamb waves refer to the elastic waves in a thin plate (the planar dimensions are far greater than the thickness and the wavelength is on the order of the plate thickness) that compulsorily requires upper and lower boundaries to maintain continuous propagation of the wave. Lamb waves include symmetric and anti-symmetric modes, denoted by S_i and A_i, respectively, in what follows, with subscript i being the wave order starting from 0.

During propagation, upon encountering an irregularity or inhomogeneity such as structural damage or a boundary, Lamb waves can be modulated to a certain extent, accompanying wave scattering (e.g. reflection, transmission, refraction and diffraction) and manifesting arrival delay of a particular wave mode, reduction in signal amplitude, energy dissipation, mode conversion, etc. For instance, interaction of the first-order symmetric mode, S_0, with delamination generates new wave modes including the first-order shear horizontal (SH) mode, denoted by SH_0, and the first-order anti-symmetric mode, A_0, in addition to some deferral of arrival of the original S_0 mode and pronounced reduction in signal magnitude. Moreover, differences in location and severity of damage produce unique scattering phenomena. The above features cause Lamb waves to be examined as a means of establishing

cost-effective damage identification tools [15–23]. Some additional benefits from using Lamb waves for detecting damage of composite structures are noteworthy [24]. Firstly, since Lamb waves can propagate a relatively long distance even in materials with high attenuation ratio such as composites, a large area of the composite structure can be inspected with a few transducers of a low granularity. Secondly, internal damage (e.g. delamination) can be detected like that on the surface (e.g. crack), by exploiting the different modes of Lamb waves (S_i and A_i modes dominate the in-plane and out-of-plane motion of the particles in plate, respectively), ensuring a full inspection coverage for the composite structures.

2.2. Conventional approach: damage triangulation using time-of-flight (ToF) of Lamb wave signal

Consider a sensor network surface-mounted on or embedded in a composite laminate, consisting of N sensors, denoted by P_i ($i = 1, 2, \ldots, N$), as seen in figure 1(a). The sensing path, in which P_m serves as the actuator and P_n as the sensor, is symbolized by P_m–P_n hereinafter. Focusing on an actuator arbitrarily selected in the network, P_i, a coordinate system is introduced where actuator P_i is at the origin. The structural damage, if any, is presumed to be at (x, y) (coordinates of the damage centre). Referring to figure 1(b), in such a coordinate system, it has the following geometric relationship [25]:

$$\frac{L_{\text{A–D}}}{V_{S_0}} + \frac{L_{\text{D–S}}}{V_{\text{SH}_{0-\text{damage}}}} - \frac{L_{\text{A–S}}}{V_{S_0}} = T_{i-j},$$
$$(j = 1, 2, \ldots, N \text{ but } j \neq i) \qquad (1a)$$

$$L_{\text{D–S}} = \sqrt{\left(x - x_j\right)^2 + \left(y - y_j\right)^2}, \qquad L_{\text{A–D}} = \sqrt{x^2 + y^2},$$
$$L_{\text{A–S}} = \sqrt{x_j^2 + y_j^2} \qquad (1b)$$

where $L_{\text{A–D}}$, $L_{\text{D–S}}$, and $L_{\text{A–S}}$ represent the distances between actuator P_i and the damage centre (x, y), the damage centre and the jth sensor (P_j), and actuator P_i and sensor P_j, respectively. (x_j, y_j) are the coordinates of sensor P_j in the coordinate system with P_i being the origin. $V_{\text{SH}_{0-\text{damage}}}$ and V_{S_0} are the velocities of the damage-induced SH_0 mode (converted from the incident S_0 as discussed in section 2.1) and the incident S_0, respectively. T_{i-j} denotes the *time-of-flight* (ToF) extracted from sensing path P_i–P_j, where ToF is defined as the time lag from the moment at which the sensor catches the incident wave to the moment at which the same sensor catches the damage-scattered wave, and in this discussed case it is the time lag between the damage-reflected SH_0 mode after mode conversion and incident S_0. The solutions to equation (1a) configure an ellipse-like locus of root (note that, mathematically, it is not exactly an ellipse), implying all the possible locations of damage in the structure, which are the perspective from the sensing path, P_i–P_j, which creates such a locus.

Taking into account one other sensing path rendered by the sensor network and repeating the above analysis, a non-linear equation group, consisting of two equations established by two sensing paths, respectively, can be created, which involves two unknown damage parameters, (x, y). Each equation in

(a)

(b)
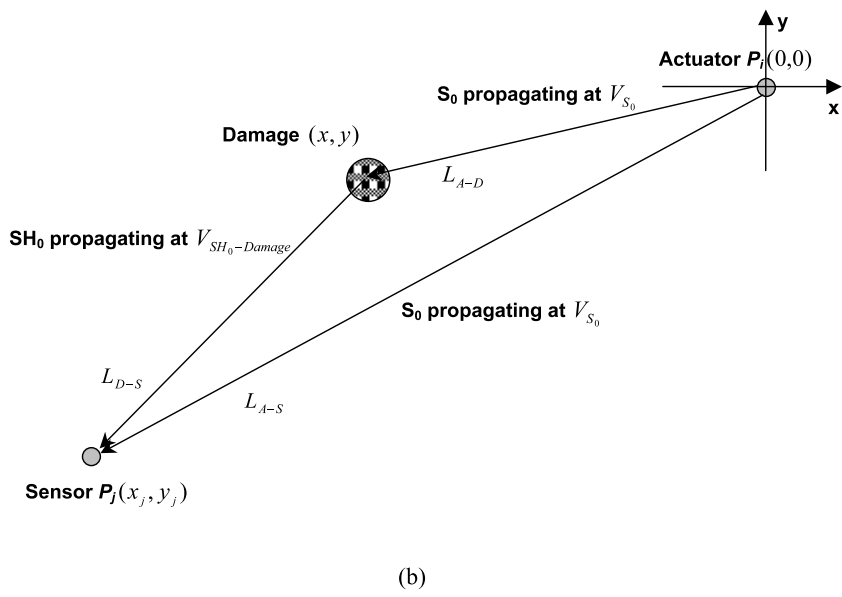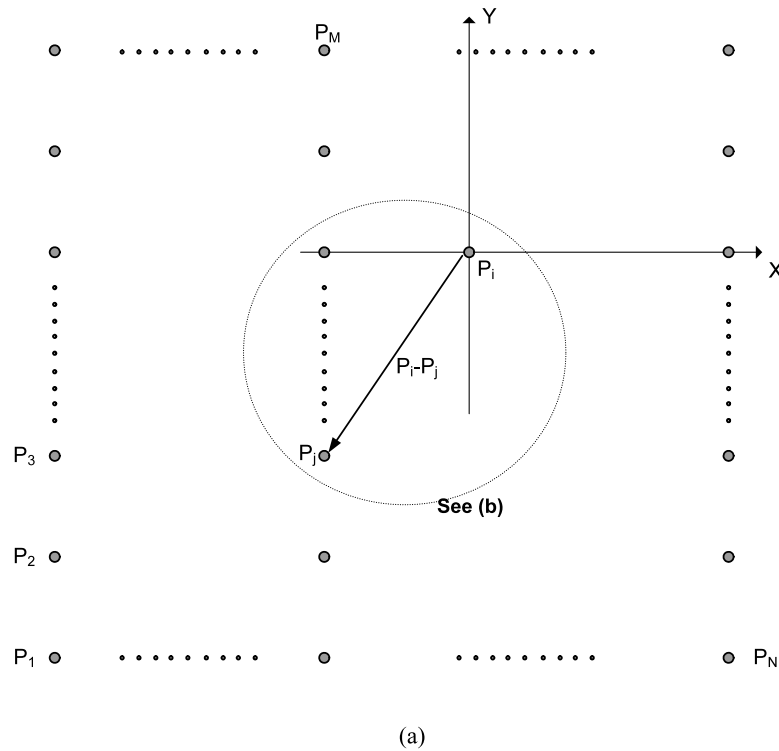
Figure 1. (a) A sensor network consisting of *N* sensors; (b) relative positions of the damage at (x, y), actuator P_i at $(0, 0)$, and sensor P_j at (x_j, y_j).

the group contributes a locus of root and two loci lead to an intersection which is the common belief from two sensing paths as to the location of damage. Most of the ToF-based approaches [17, 20, 25] triangulate structural damage using such a philosophy, to provide definitive damage parameters and location coordinates in particular.

It should be particularly emphasized herein that, in order to predict damage in terms of the probability of its occurrence at a certain spatial position of the structure, *no* attempt was made in this study to triangulate the damage by seeking the intersections of two loci like those conventional approaches did.

3. Damage prediction in terms of occurrence probability

Distinct from the above-briefed conventional triangulation approaches to locate damage with definitive damage parameters (such as location coordinate of damage centre), a probability-based prediction algorithm in conjunction with an active sensor network was developed, which was motivated by the recognition that damage identification is an exercise to *predict* or *estimate* damage, and it is ideal to present the prediction results in terms of the *probability* of damage occurrence across the entire structure under interrogation.

To establish the probability of damage occurrence at all the spatial positions of the structure, the inspection area (the area enclosed by the sensors of a sensor network) was virtually and evenly meshed. It is axiomatic that, if mesh nodes rightly locate on a certain locus of root attained with the approach described in section 2, these mesh nodes have the highest degree of probability (100%) to be contained in a damage event, which is from the perspective of the sensing path that produces such a locus; while for other mesh nodes of the structure, the further the distance to the locus, the lower the probability that damage exists at these nodes, which is also from the perspective of the same sensing path. Therefore, the distance from a certain spatial mesh node of the structure to any of the loci can be associated with the probability of damage existence at this node. The physical intuition behind this is that a defect would cause the most significant signal changes in the direct wave path, and that the degree of signal change would decrease, if the defect were away from the sensing path.

Without loss of generality, consider a square panel and the inspection area virtually using $K \times K$ nodes, as shown schematically in figure 2(a). The shortest distances from all mesh nodes to all the loci of root attained were calculated. By way of illustration, such distances for two arbitrarily selected spatial mesh nodes, L_m and L_n, of the structure with regard to two loci, also arbitrarily selected, are shown in figure 2(b). To quantify the probabilities at all the spatial nodes in relation to all the loci, a *cumulative distribution function* (CDF) [26], $F(z)$, was introduced, defined as

$$F(z) = \int_{-\infty}^{z} f(z_{ij}) \, dz_{ij} \qquad (2)$$

where $f(z_{ij}) = \frac{1}{\sigma_{ij}\sqrt{2\pi}} \exp[-\frac{z_{ij}^2}{2\sigma_{ij}^2}]$ is the *Gaussian distribution function*, representing the probability density function (PDF) of damage occurrence at node L_i ($i = 1, \ldots, K \times K$), established by sensor P_j ($j = 1, \ldots, N$ for the sensor network consisting of N sensors). $z_{ij} = ||\chi_i - \mu_{ij}||$, where χ_i is the location vector of mesh node L_i and μ_{ij} is the location vector of the point on the locus that has the shortest distance to L_i. σ_{ij} is the standard variance.

4. Distributed active sensor network

In the above process, it can be seen that a number of sensors, appropriately distributed, play a vital role to collect information as to damage and then establish probabilities of damage occurrence throughout the whole structure. These sensors form a distributed sensor network, much akin to the nerve cells of human beings. Basically, an ideal sensor for smart structures with a capacity of self-health monitoring should meet requirements including (i) veridical acquisition of changes in local or global structural responses, (ii) faithful delivery of the above captured changes, (iii) possibly less intrusion to host structure, (iv) endurance under general working conditions with a service life of no less than the host structure, and (v) ease in handling, attachment, integration, and operation. There are many options of sensing devices including ultrasonic probe, acoustic emission (AE) sensor, magnetic

(a)

(b)
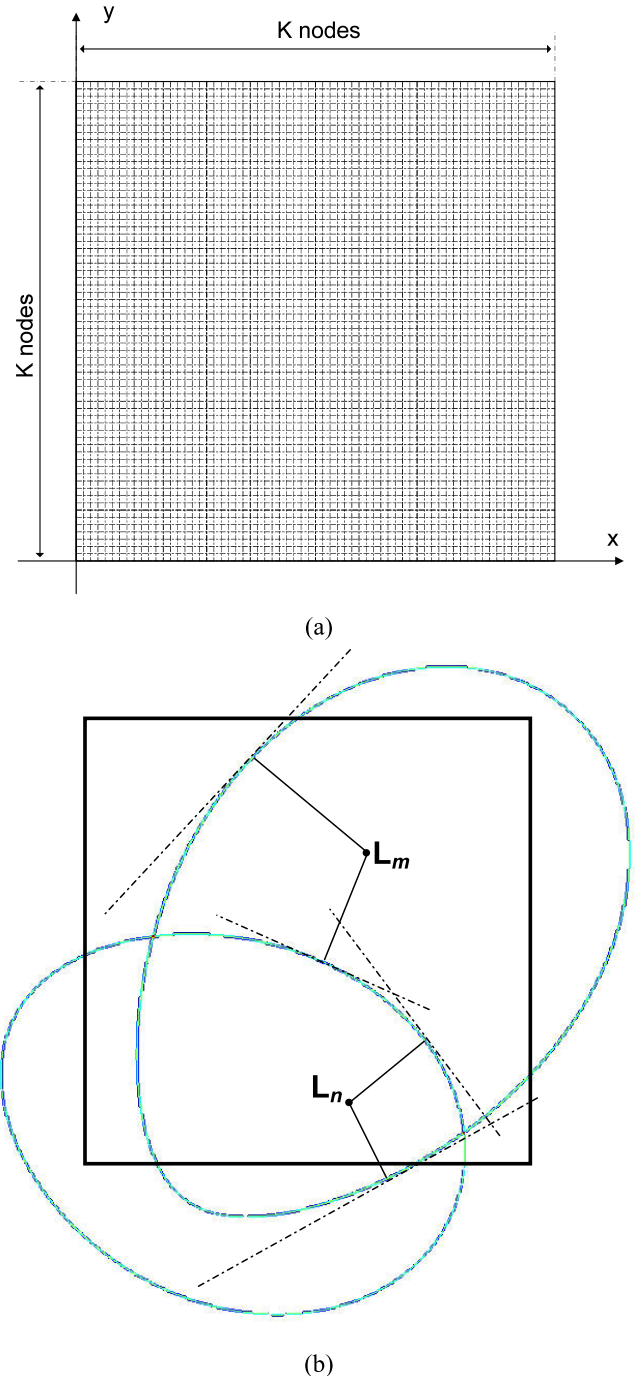
Figure 2. (a) A square panel meshed virtually and evenly using $K \times K$ nodes; (b) the distances of two arbitrarily selected spatial nodes of the panel, L_m and L_n, with regard to two loci.

sensor, eddy-current transducer, accelerometer, strain gauge, laser interferometer, optical fibre, electro-magnetic acoustic transducer (EMAT), etc. In particular, the piezoelectric lead zirconate titanate (PZT) elements are very suitable to integrate into a host structure as an *in situ* actuator or sensor, as a result of their low mass, good mechanical strength, wide frequency band, low power consumption and acoustic impedance, and low cost. In terms of its dual piezoelectric effects, a PZT element can be designed to generate a diagnostic Lamb wave signal and acquire response signals. A number

Table 1. Material properties of plain woven fabric used for experimental validation.

0° tensile modulus (GPa)	0° compressive modulus (GPa)	Fibre volume percentage (%)	Poisson's ratio	Density (g cm^{-3})
59.9–62.0	55.1–57.9	62	0.2 (fibre) 0.35 (resin)	1.78 (fibre) 1.22 (resin)

of spatially distributed PZT elements, performing local data acquisition and then 'communicating' with each other, can configure an active sensor network to provide chunks of information [27–29]. With sensors acting cooperatively, a PZT sensor network insures the completeness and reliability of signal acquisition. In a PZT sensor network, any two PZT elements form an actuator–sensor pair (sensing path), to perceive the damage near the sensing path by establishing the root of locus aforementioned. In other words, distributed sensors of the sensor network form their individual beliefs that represent their own interpretation of data or 'the world' they sense.

5. Image fusion

For every single sensing path provided by the distributed active sensor network, the possibilities of damage occurrence were quantified at all mesh nodes of the structure in terms of $F(z)$, equation (2), leading to an image if we use a grey-scale to indicate the value of probabilities. In such an image, each pixel exclusively corresponds to a spatial mesh node of the structure, sharing the same coordinates.

Individual images contain, in addition to damage-scattered waves, unwanted features such as noise, multiple reflections from boundaries, multi-wave modes, etc. Under such a circumstance, the damage-scattered waves may not be fully exhibited in an individual image. To preserve and then accentuate the common beliefs as to possible damage from all the sensors of the sensor network, the image fusion technique was employed. Literally, image fusion in conjunction with multiple sensors is the process of combining two or more input images obtained from different sources (e.g. different sensors of a sensor network) into a resulting image, so as to achieve specific purposes such as enhanced signal-to-noise ratio (SNR) or obvious damage size. Basically, an image fusion process is utilized to increase the robustness and reliability of an identification exercise by reducing imprecision, uncertainties and incompleteness as much as possible, and most importantly to draw a *decision* or *consensus* by combining all the *beliefs* of individual sensors. In particular, for damage identification, image fusion aims at establishing a visual description of the overall health status of structures by aggregating images perceived by all the sensors. The fusion can therefore be seen as a route from perceptions of individual sensors to ultimate consensus of the sensor network.

During implementation of the image fusion in the study, images were fused by first considering one pixel at a time and determining the pixel value of the resulting image in terms of the corresponding pixels of every single image established by individual sensors, while neighbouring pixels were not considered. Subsequently, the above analysis was

applied to other pixels of the resulting image. In practice, several strategies of image fusion are possible, and a detailed discussion on the selection of an appropriate fusion scheme can be referred to the authors' previous work [30]. In the present study, the image fusion scheme based on the *generalized mean* was adopted. The generalized mean, also known as the *power mean*, is an abstraction of the quadratic, arithmetic, geometric, and harmonic means. Amongst different means, the geometric mean has been demonstrated particularly effective to produce a resulting image by considering information from all input images, i.e. perceptions established by all the sensors. The geometric mean, mean$_{geo}$, in mathematics is a type of mean or average that indicates the central tendency or typical value of a set of numbers, defined as, for a data set [$a_1, a_2, \ldots, a_n$] [31],

$$\mathrm{mean}_{geo} = \left(\sum_{i=1}^{n} a_i \right)^{\frac{1}{n}} = \sqrt[n]{a_1 \cdot a_2 \cdots a_n}. \qquad (3)$$

The geometric mean can be understood in terms of geometry as follows. The geometric mean of two numbers, a and b, is simply the side length of the square whose area is equal to that of a rectangle with side lengths a and b. Similarly, the geometric mean of three numbers, a, b, and c, is the side length of a cube whose volume is the same as that of a rectangular prism with side lengths equal to the three given numbers.

6. Experimental validation

6.1. Sample preparation and test

To validate the proposed approach, three $[(\pm45)/(0/90)]_{4s}$ woven fabric laminates (T650/F584) with properties listed in table 1 were fabricated, measuring $500 \times 500 \times 3.6$ mm^3 each. One of these three laminates was kept intact as the benchmark; one contains a piece of circular delamination ($\varnothing 40$ mm), figure 3(a), and the last one contains two pieces of delamination ($\varnothing 30$ mm and $\varnothing 60$ mm, respectively), figure 3(b), by inserting thin Teflon® films before autoclave processing. Each of these laminates was embedded with an active sensor network consisting of 12 PZT wafers (PI®-151, $\varnothing 10$ mm and 0.2 mm in thickness). The PZT wafers were numbered clockwise with P_i ($i = 1, 2, \ldots, 12$), as seen in figure 3. All the PZT wafers were thoroughly protected by a pre-coating layer of epoxy to prevent the anode and cathode of the PZT coming into contact with carbon fibres in the autoclave stage of the manufacturing process. The laminates were then instrumented with a signal generation and data acquisition system [25], with which the Hanning-window-modulated five-cycle sinusoid tonebursts at a central frequency of 250 kHz and with a peak–peak amplitude of 50 V were generated and

(a)

(b)
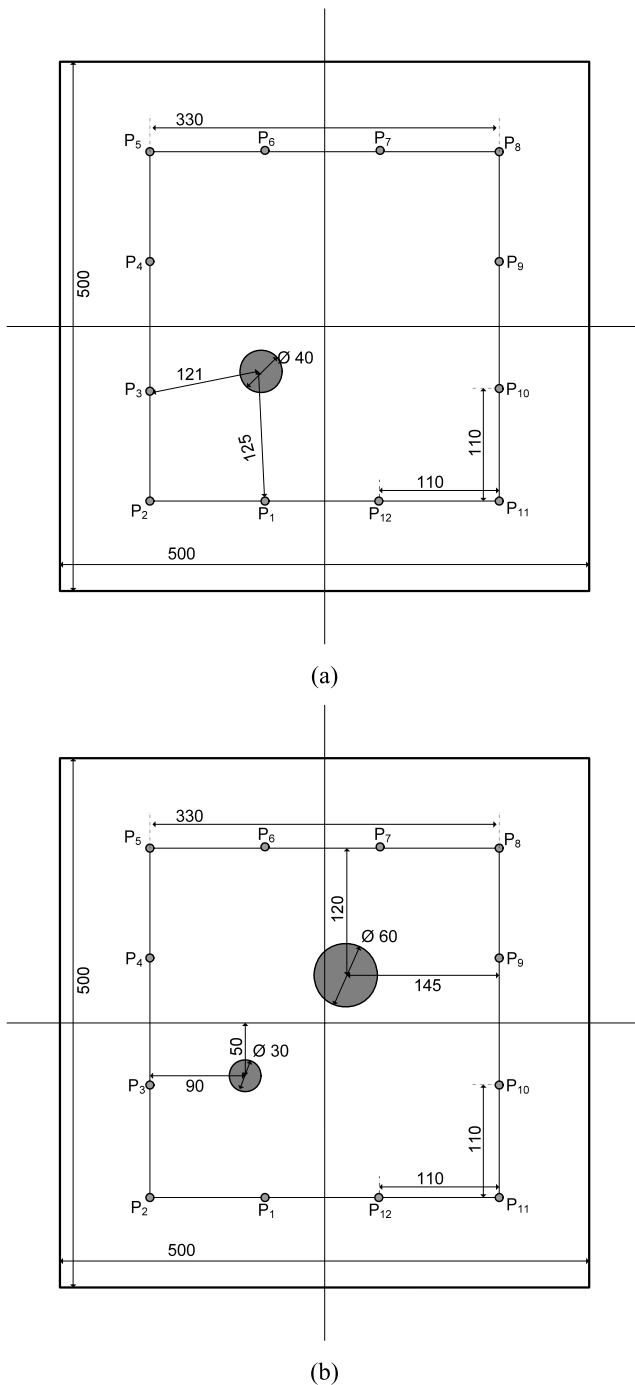
Figure 3. Schematic diagram of two CF/EP composite laminates for experimental validation, containing (a) single and (b) dual delamination, respectively (unit: mm).

applied in turn to each PZT wafer of the sensor network to produce diagnostic Lamb waves, and the Lamb wave signals containing the wave components scattered by damage, if any, were captured via all the available sensing paths in the sensor network.

One representative signal, captured via sensing path P_7–P_9 in the laminate containing dual delamination, is shown in figure 4, from which the damage-induced SH_0 mode (converted from the incident S_0 upon interaction with delamination) can
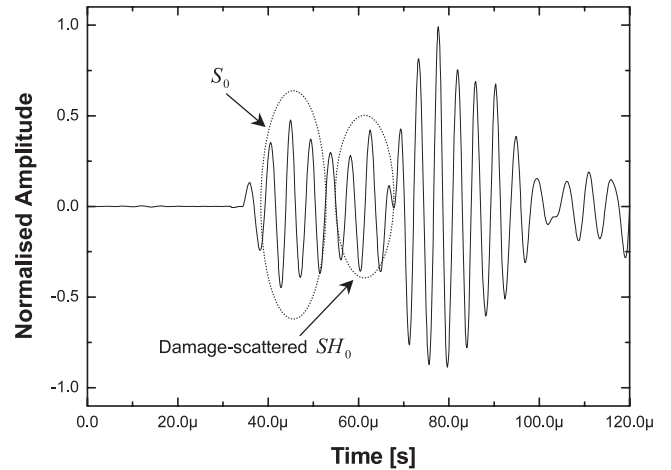
Figure 4. A representative signal, captured via sensing path P_7–P_9 in the laminate containing dual delamination.

be observed clearly. The measured velocity of the S_0 mode from the signal is near 5000 m s^{-1} in the quasi-isotropic woven fabric laminates.

6.2. Damage imaging

Three laminates were meshed virtually. With ToFs extracted from captured Lamb wave signals, probabilities as to damage existence at all the spatial nodes across the laminates were established in terms of equation (2) and delineated by a grey-scaled contour diagram for each sensing path. Representatively, two such diagrams, contributed by two sensing paths arbitrarily selected from the sensor network, are displayed in figure 5, where the lighter the grey-scale the greater the possibility of damage occurrence at these pixels. The established probabilities at all the spatial nodes of each laminate were then fused using the geometric mean aforementioned, and the resulting images for two damaged laminates are presented in figure 6.

If 80% of the maximum value of the probabilities shown in the diagrams was set as the threshold to draw a conclusion that damage occurs, one and two regions of probabilities over such a threshold are clearly observed in figure 6, indicated with dotted circles, respectively. It reveals that one and two damage events take place in laminates, respectively. For comparison, the real delamination of two laminates was highlighted with solid circles in the figures. Interestingly, the areas of these dotted-line-restricted regions are similar to those of actual delamination ($\varnothing$40 mm for laminate containing single delamination; $\varnothing$30 mm, $\varnothing$60 mm for laminate containing dual delamination). The capacity of the approach to pinpoint the rough size of the damage is based on the fact that only those paths near the delamination zone show a significant signal change, and inversely the approximate damage size can be estimated by ascertaining the area which contains sensing paths that are phenomenally different to their corresponding benchmark signals. In these diagrams, the coordinates correspond to the real locations of mesh nodes of the laminates, therefore offering an intuitional depiction of all possible damage instances in the structure under inspection.

(a)

(b)
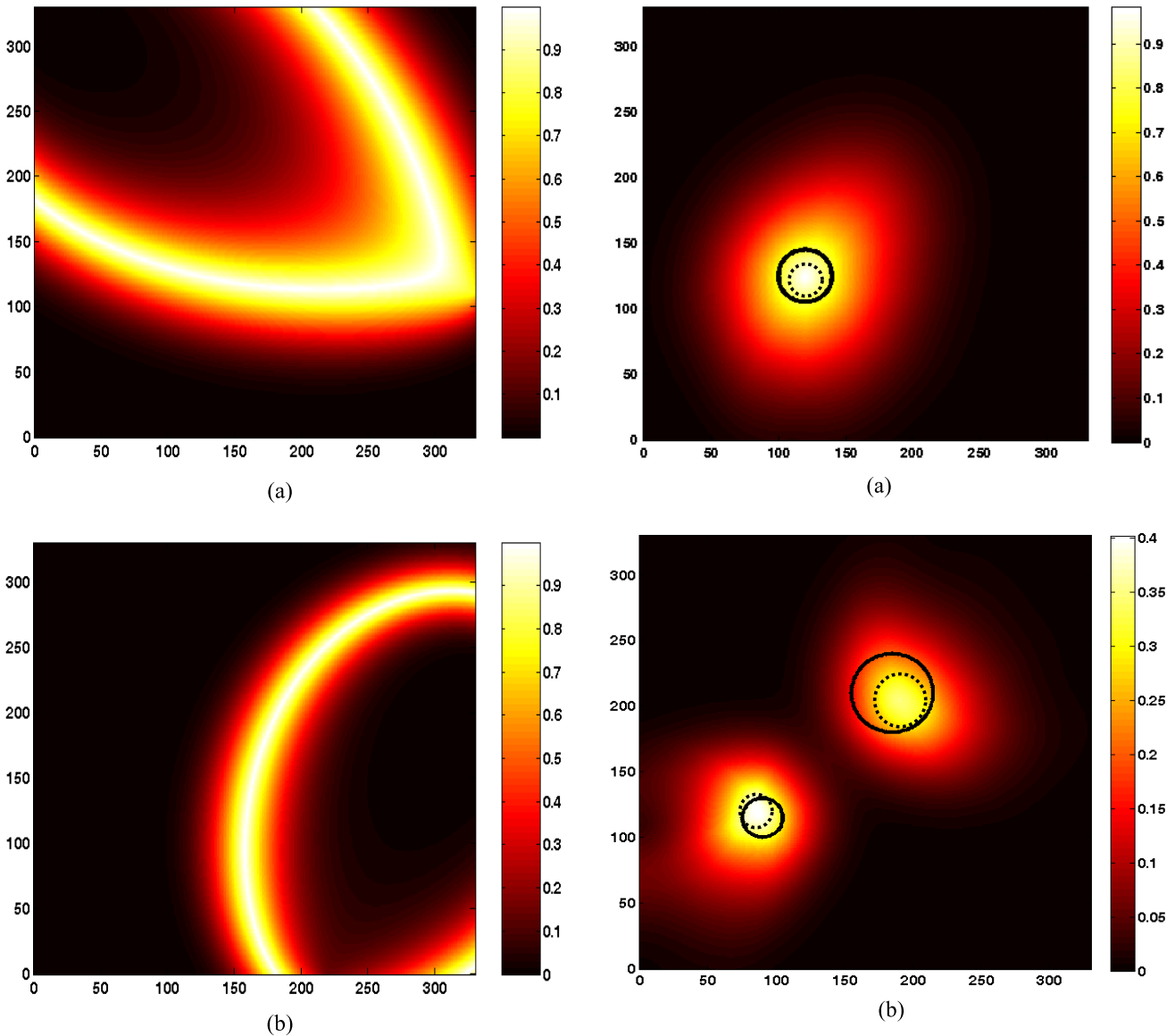
Figure 5. Probability diagrams established by sensing paths of (a) P_{10}–P_5 in laminate containing single delamination; (b) P_{12}–P_9 in laminate containing dual delamination (diagrams showing the inspection area only, i.e. the area enclosed by 12 sensors; unit of both coordinate axes: mm).

(a)

(b)

Figure 6. Prediction results for laminates containing (a) single and (b) dual delamination using the imaging fusion (diagrams showing the inspection area only; unit of both coordinate axes, mm; solid circles, actual delamination in laminates; dotted circles, predicted delamination if 80% of the maximum value of the probabilities is set as the threshold).

It is noteworthy that the highest probability in figure 6(b) for the laminate containing dual delamination (less than 40%) is much lower than that in figure 6(a) for the laminate bearing single delamination. This can be attributed to the nature of $F(z)$, equation (2), in which an exponential function was used to define the probabilities at spatial nodes. As a consequence, from the perspective of a sensor which established the probabilities as to damage occurrence across the structure, the probabilities at regions far away from it would become very low. That is to say, in terms of $F(z)$, sensors of a sensor network only perceive the damage near them. When fused, the overall probability at a particular pixel of the resulting image could become significantly lower than the probabilities at the same pixel location of individual input images.

7. Conclusion

Bearing in mind that damage identification is an exercise of *predicting* damage and the results should accordingly be delivered in terms of probability, a probability-based imaging approach was developed based on Lamb waves. Prediction of all the possible damage instances of the structure under inspection was achieved by fusing perceptions from individual sensors of an active PZT sensor network, which was then calibrated by greyscale in an intuitional contour map related to the probability of damage occurrence. As validation, the approach was employed to identify single and dual delamination in CF/EP laminates, respectively, and the results, represented in intuitional images, showed good identification capacity of the approach.

References

[1] Pora J 2003 Advanced materials and technologies for A380 structure: technology platform for future developments http://www.content.airbusworld.com

[2] Talbot D 2003 Boeing's flight for survival *Technology Review* September issue

[3] Montalvão D, Maia N M M and Ribeiro A M R 2006 A review of vibration-based structural health monitoring with special emphasis on composite materials *Shock Vib. Dig.* **38** 295–324

[4] Achenbach J D 2000 Quantitative nondestructive evaluation *Int. J. Solids Struct.* **37** 13–27

[5] Boller C 2001 Ways and options for aircraft structural health management *Smart Mater. Struct.* **10** 432–40

[6] Gray J and Tillack G-R 2001 X-ray imaging methods over the last 25 years—new advances and capabilities *Review of Progress in Quantitative Nondestructive Evaluation* vol 20, ed D O Thompson and D E Chimenti, pp 16–32

[7] Staszewski W J, Boller C and Tomlinson G R 2004 *Health Monitoring of Aerospace Structures: Smart Sensor Technologies and Signal Processing* (New York: Wiley)

[8] Wang C H, Rose J T and Chang F-K 2004 A synthetic time-reversal imaging method for structural health monitoring *Smart Mater. Struct.* **13** 415–23

[9] Michaels J E and Michaels T E 2006 Enhanced differential methods for guided wave phased array imaging using spatially distributed piezoelectric transducers *Review of Progress in Quantitative Nondestructive Evaluation* vol 25, ed D O Thompson and D E Chimenti, pp 837–44

[10] Ihn J-B and Chang F-K 2008 Pitch–catch active sensing methods in structural health monitoring for aircraft structures *Struct. Health Monit.* **7** 5–19

[11] Konstantinidis G, Wilcox P D and Drinkwater B W 2007 An investigation into the temperature stability of a guided wave structural health monitoring system using permanently attached sensors *IEEE Sensors J.* **7** 905–12

[12] Michaels J E and Michaels T E 2007 Guided wave signal processing and image fusion for *in situ* damage localization in plates *Wave Motion* **44** 482–92

[13] Zhao X, Gao H, Zhang G, Ayhan B, Yan F, Kwan C and Rose J L 2007 Active health monitoring of an aircraft wing with embedded piezoelectric sensor/actuator network: I. Defect detection, localization and growth monitoring *Smart Mater. Struct.* **16** 1208–17

[14] Chiu W K, Koh Y L, Galea S C and Rajic N 2000 Smart structure application in bonded repairs *Compos. Struct.* **50** 433–44

[15] Rose J L 1999 *Ultrasonic Waves in Solid Media* (New York: Cambridge University Press)

[16] Guo N and Cawley P 1993 The interaction of Lamb waves with delaminations in composite laminates *J. Acoust. Soc. Am.* **94** 2240–6

[17] Wang C S and Chang F-K 1999 Built-in diagnostics for impact damage identification of composite structures *Structural Health Monitoring* 2 edn, ed F-K Chang (Lancaster: Technomic Publishing) pp 613–21

[18] Badcock R A and Birt E A 2000 The use of 0-3 piezocomposite embedded Lamb wave sensors for detection of damage in advanced fibre composites *Smart Mater. Struct.* **9** 291–7

[19] Monkhouse R S C, Wilcox P, Lowe M J S, Dalton R P and Cawley P 2000 The rapid monitoring of structures using interdigital Lamb wave transducers *Smart Mater. Struct.* **9** 304–9

[20] Lemistre M and Balageas D 2001 Structural health monitoring system based on diffracted Lamb wave analysis by multiresolution processing *Smart Mater. Struct.* **10** 504–11

[21] Kessler S S, Spearing S M and Soutis C 2002 Damage detection in composite materials using Lamb wave methods *Smart Mater. Struct.* **11** 269–78

[22] Park H W, Sohn H, Law K H and Farrar C R 2007 Time reversal active sensing for health monitoring of a composite plate *J. Sound Vib.* **302** 50–66

[23] Ghoshal A, Martin W N and Schulz M J 2002 Simulation of asymmetric Lamb wave propagation for health monitoring *Proc. 1st European Workshop on Structural Health Monitoring (Paris, July 2002)* ed D Balageas, pp 365–73

[24] Chimenti D E 1997 Guided waves in plates and their use in materials characterization *Appl. Mech. Rev.* **50** 247–84

[25] Su Z, Wang X, Chen Z, Ye L and Wang D 2006 A built-in active sensor network for health monitoring of composite structures *Smart Mater. Struct.* **15** 1939–49

[26] Ang A H-S and Tang W H 1975 *Probability Concepts in Engineering Planning and Design* (New York: Wiley) pp 170–203

[27] Lemistre M B and Balageas D L 2003 A hybrid electromagnetic acousto-ultrasonic method for SHM of carbon/epoxy structures *Struct. Health Monit.* **2** 153–60

[28] Qing X, Kumar A, Zhang C, Gonzalez I F, Guo G and Chang F-K 2005 A hybrid piezoelectric/fiber optic diagnostic system for structural health monitoring *Smart Mater. Struct.* **14** 98–103

[29] Giurgiutiu V 2008 *Structural Health Monitoring with Piezoelectric Wafer Active Sensors* (Boston, MA: Elsevier Academic)

[30] Su Z, Wang X, Cheng L, Yu L and Chen Z 2008 On selection of data fusion schemes for structural damage evaluation *Struct. Health Monit.* at press

[31] Hardy G H, Littlewood J E and Pólya G 1988 *Inequalities* 2nd edn (New York: Cambridge University Press)